



● *Original Contribution*

**PULSED HIGH INTENSITY FOCUSED ULTRASOUND MEDIATED  
 NANOPARTICLE DELIVERY: MECHANISMS AND EFFICACY IN  
 MURINE MUSCLE**

BRIAN E. O'NEILL,\*<sup>†</sup> HOWARD VO,\* MARY ANGSTADT,\* KING P. C. LI,\* TIM QUINN,<sup>†</sup>  
 and VICTOR FRENKEL\*

\*Diagnostic Radiology Department, Clinical Center, National Institute of Health, Bethesda, MD, USA; and

<sup>†</sup>Materials Reliability Division, National Institute of Standards and Technology, Boulder, CO, USA

(Received 21 April 2008; revised 5 August 2008; in final form 19 September 2008)

**Abstract**—High intensity focused ultrasound (HIFU) is generally thought to interact with biological tissues in two ways: hyperthermia (heat) and acoustic cavitation. Pulsed mode HIFU has recently been demonstrated to increase the efficacy of a variety of drug therapies. Generally, it is presumed that the treatment acts to temporarily increase the permeability of the tissue to the therapeutic agent, however, the precise mechanism remains in dispute. In this article, we present evidence precluding hyperthermia as a principal mechanism for enhancing delivery, using a quantitative analysis of systemically administered fluorescent nanoparticles delivered to muscle in the calves of mice. Comparisons were carried out on the degree of enhancement between an equivalent heat treatment, delivered without ultrasound, and that of the pulsed-HIFU itself. In the murine calf muscle, Pulsed-HIFU treatment resulted in a significant increase in distribution of 200 nm particles ( $p < 0.016$ ,  $n = 6$ ), while the equivalent thermal dose showed no significant increase. Additional studies using this tissue/agent model also demonstrated that the pulsed HIFU enhancing effects persist for more than 24 h, which is longer than that of hyperthermia and acoustic cavitation, and offers the possibility of a novel third mechanism for mediating delivery. (E-mail: [vfrenkel@cc.nih.gov](mailto:vfrenkel@cc.nih.gov)) Published by Elsevier Inc. on behalf of World Federation for Ultrasound in Medicine & Biology.

**Key Words:** Pulsed-high intensity focused ultrasound, Nanoparticle delivery, Hyperthermia, Cavitation, Radiation force.

**INTRODUCTION**

The vast majority of therapeutic applications of high intensity focused ultrasound (HIFU) presently employ relatively long, continuous exposures for thermally ablating tissue (Kennedy 2005). By comparison, pulsed exposures generate noncontinuous energy deposition, which reduces the temporal average intensity and buildup of heat (Miller and Song 2003). Preliminary evidence has indicated that pulsed exposures can induce acousto-mechanical effects in tissues due to mechanisms such as radiation forces and, consequently, enhance the local permeability of the exposed tissue (Frenkel et al. 2005; O'Neill et al. 2005). For example, pulsed-HIFU (p-HIFU) exposures in tumors, followed by either local or systemic administrations, have been

shown to enhance the delivery of a high-molecular weight fluorophore (Yuh et al. 2005), fluorescently labeled polystyrene nanoparticles (Frenkel et al. 2006a), plasmid DNA (Dittmar et al. 2005; Quijano et al. 2005) and monoclonal antibodies (Khaibullina et al. 2008) in a nondestructive manner (Dittmar et al. 2005; Frenkel et al. 2006a; Khaibullina et al. 2008). Additional *in vitro* studies demonstrated that the exposures could improve delivery of tissue plasminogen activator (tPA) to blood clots (Stone et al. 2007) and, consequently, increase their rate of thrombolysis *in vitro* (Frenkel et al. 2006b) and *in vivo* (Stone et al. 2007) when compared to treatments with tPA alone.

While the therapeutic benefits of p-HIFU are well established, the mechanism is, at this time, far from certain. HIFU is usually thought to interact with tissue in two prominent ways; by heating and by acoustic cavitation (O'Brien et al. 2007). Weak mechanical forces, such as radiation or shear forces, are sometimes discussed as a third possibility (Frenkel et al. 2005, 2006b; O'Neill et

Address correspondence to: Victor Frenkel, Ph.D., Diagnostic Radiology Department, Clinical Center, National Institutes of Health, Building 10, Room 1N306a, 10 Center Drive, Bethesda, MD, USA 20892. E-mail: [vfrenkel@cc.nih.gov](mailto:vfrenkel@cc.nih.gov)

al. 2005). The purpose of the research presented here is to investigate the possibility of a predominantly thermal mechanism for enhancing delivery. Past efforts have shown that the temperature rise during our standard p-HIFU treatment generally peak a little less than 5°C above ambient for tumors, or 42°C when using a 37°C bath (Frenkel et al. 2006a; Patel et al. 2008). The hyperthermia literature suggests that this temperature may indeed be sufficient for biologically relevant effects, such as enhancing extravasation of nanoparticles (Kong et al. 2001). However, hyperthermia treatments normally last an hour or more, whereas, during a p-HIFU treatment, a single exposure zone reaches this temperature for less than 2 min. Lower temperatures are reached during p-HIFU treatment of neighboring regions; however, the biological significance of these temperatures is much less. This fact is modeled by the conversion of the temperatures to thermal doses (Sapereto and Dewey 1984), which represent the cumulative effect of heat on tissue. In this study, the delivery of fluorescent nanoparticles (NP) due to p-HIFU treatment at two different bath temperatures are compared to a nonultrasonic heat source reaching the same peak temperature and delivering an overall greater thermal dose. Investigations are also carried out on the reversibility of the enhancing effects and the potential role of acoustic cavitation.

## MATERIALS AND METHODS

### *HIFU treatment*

A custom, image-guided HIFU system was used for our study, modified from a Sonoblate® 500 (Focus Surgery; Indianapolis, IN, USA). The probe possesses both a therapeutic (1 MHz, focal length 4 cm) transducer and a co-axial (10 MHz) imaging transducer. The concave therapeutic transducer has a diameter of 5 cm; the imaging transducer's aperture is 0.8 cm. The therapeutic transducer has a maximum available total acoustic power (TAP) of 120 W, calibrated by use of the radiation force balance technique. The focusing factor of the therapy transducer is approximately  $1.3 \times 10^3$ , where simulations of the focal zone indicated that it was ellipsoid in shape with an axial length (−3 dB) of 7.2 mm and a radial diameter (−3 dB) of 1.38 mm. A single exposure consists of 100 pulses at a pulse repetition frequency of 1 Hz, 5% duty cycle and a peak TAP of 40 W, unless otherwise specified. For these standard exposures, the spatial averaged intensity was calculated to be  $2685 \text{ W cm}^{-2}$  and the peak negative pressure amplitude to be 8.95 MPa.

All animal work was performed according to an approved animal study protocol and in compliance with NIH, Clinical Center Animal Care and Use Committee guidelines. Female C3H mice, at least 8 wk in age, were used for all experiments. Treatments were carried out as previously

described (Dittmar et al. 2005; Frenkel et al. 2006a; Yuh et al. 2005). Briefly, anesthetized mice (2% isoflurane; O<sub>2</sub> 1L/h) were immersed, secured in an upright position, in a degassed water bath, where the head of the mouse was above the water line in an anesthesia nose cone. Targeting of the calf was achieved by imaging with the 10 MHz imaging probe. A region of the calf muscle was treated with multiple exposures on a  $2 \times 3$  square grid, with 2 mm separation between points. The time required for the probe to move from exposure to exposure was approximately 1 s. Our standard treatments (HIFU37) are carried out with the bath temperature nominally controlled to 37°C. The “low temperature” (HIFU34) treatments were carried out with the bath temperature reduced to 34°C.

### *Determination of the pulsed-HIFU equivalent thermal dose*

The thermal dose supplied by p-HIFU exposures was determined by measuring temperatures in the tissue by use of a pair of 30 Ga hypodermic thermocouples (Omega Engineering Inc., Stamford, CT, USA). Standard conditioning hardware was used to amplify the signal from the thermocouples before it was measured and displayed on the channels of a digital oscilloscope. The measurements were transferred at 0.25 s intervals to storage in a text file for later processing off-line. Temperature measuring typically began 10 to 20 s before the treatment and ended after temperature returned to less than 1°C above pretreatment levels. The use of thermocouples suffers from one major drawback, that is, the difficulty of controlling the position of the thermocouple relative to the ultrasonic beam. Unfortunately, the ultrasonic guidance built into the HIFU system has sufficient resolution for only gross localization. Typically, investigators try to set the probe so as to maximize the measured temperature, while avoiding clearly unrealistic behavior (Horder et al. 1998; Hynynen 1991). This is less than optimal, however, because the beam waist in the focal zone is quite narrow, so that even small uncertainties may potentially result in significant underestimates. On the other hand, there is reason to believe that locating the probe directly in the focal zone might well introduce errors due to extraneous heating along the metal probe itself (Clarke and ter Haar 1997).

To increase confidence in the results, we made use of measurements from several points outside of the focal zone, which were then extrapolated to estimate the peak temperature. A series of thermal trajectories, including a full cool down period, were measured during p-HIFU treatments made on a known grid near and around a single probe point (Fig. 1). Assuming the tissue is isotropic, this grid of measurements results in a sparse sampling of the spatial temperature distribution. These data were then fit to a cylindrically symmetric solution to

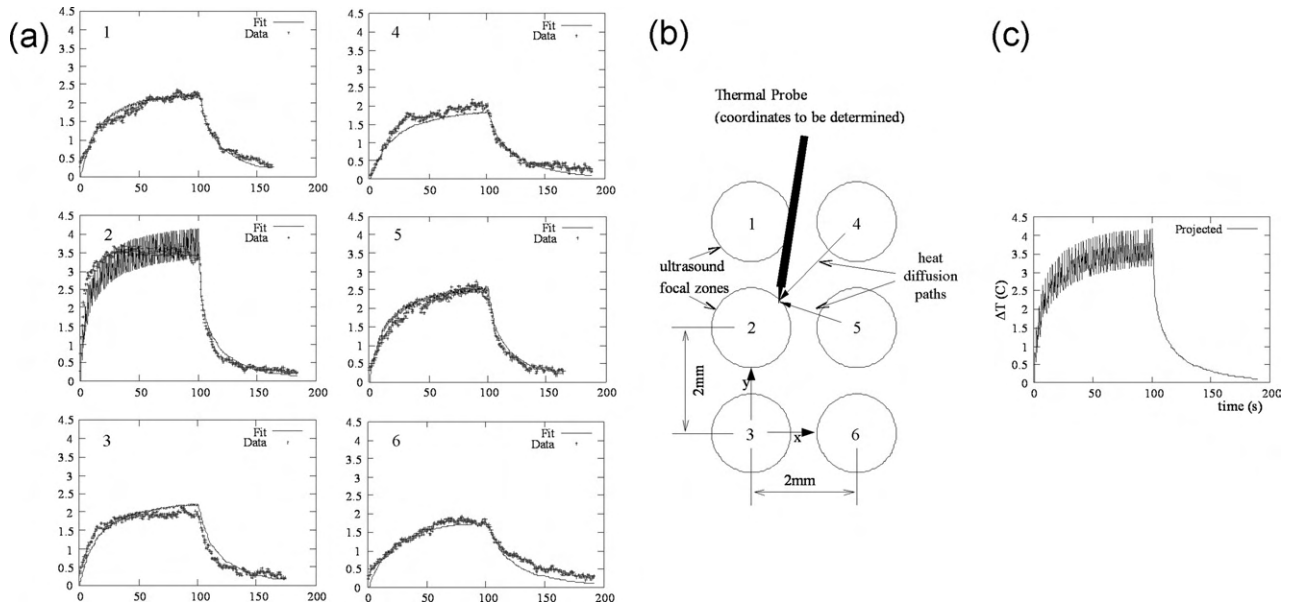


Fig. 1. Measurement of temperature at the center of the ultrasonic focus by use of an interstitial thermocouple. The probe is positioned and exposures are given at six treatment points. (a) Temperature curves at six individual treatment points ( $x$ -axis is min.;  $y$ -axis is  $^{\circ}\text{C}$ ). (b) Schematic representation of the six treatment points and their relative position to the probe, whose coordinates are unknown. (c) Projected focal zone temperature at an individual treatment point using temperature increases due to heating at neighboring sites, which are fit to the bioheat equation. Note, the graphs (1 to 6) in “a” correspond to the similarly positioned focal zones in “b”.

the bio-heat equation (Wu and Du 1990) in space and time, including the coordinates of the probe as additional fitting parameters. Peak temperatures were found to be from 3.5 to 4.5 $^{\circ}\text{C}$  above ambient. Further model details may be found in the Appendix 1.

Upon fitting the measured curves for the isolated p-HIFU raster points, it became apparent that the spatial extent of the heating was broader than originally anticipated, that is, heating from neighboring points was not insignificant (Fig. 1). During a normal treatment cycle, there was no significant cool down time between raster points, so tissue was subject to additional heating from adjacent points. To practically sample the heating due to such a treatment, a pair of thermocouples was inserted during a full treatment without cooling. Of six such measurements, two resulted in recorded temperatures spiking more than 6 $^{\circ}\text{C}$  above ambient at a single raster point, and were subsequently discarded as artifacts of direct probe heating. The others showed heating only slightly higher than the previously extrapolated value.

From the temperature versus time data, the  $t_{43}$  thermal dose was calculated by use of the formula:  $t_{43} = \int 0.25^{43-T(t)} dt$ , for temperatures between 37 and 43 $^{\circ}\text{C}$  (Sapareto and Dewey 1984). This was done for the fitted single point data, which were extrapolated to a full treatment by considering a serial contribution from nearest neighbor raster points. It was also calculated for the temperature data collected during continuous rastering, *i.e.*, no

cool down period between exposures (Table 1). The heat treatment (HT) was then set at 42 $^{\circ}\text{C}$  for 2 min (plus cool down period), to match or exceed the p-HIFU heating in terms of both temperature and thermal dose. The “low temperature” bath treatment (HIFU34) was designed to bring the peak temperatures down below 39 $^{\circ}\text{C}$ , the minimum generally thought needed for a hyperthermic effect for enhancing nanoparticle extravasation (Kong *et al.* 2001). A summary of the peak temperatures and thermal doses associated with p-HIFU and HT appear in Table 1.

Table 1. Peak temperatures and thermal doses associated with p-HIFU; comparison with HT and “low temperature” B34 targets

Measurement	Maximum Temp (measured)	Peak temp (extrapolated)	$t_{43}$ equivalent (s)
Single points	40.4	41.0	9.6
Single points	40.0	41.2	7.3
Single points	39.6	40.1	2.6
Continuous	40	-	2
Continuous	>43	-	>100
Continuous	41	-	4
Continuous	40	-	2
Continuous	>43	-	>100
Continuous	42	-	24
HT target	42	-	50
HIFU34 target	39	-	~0

### Heat treatment

The heat treatment consisted of the thermal dose described above administered by use of a heat lamp powered through a potentiometer. The lamp was placed approximately 1 cm above the target limb and its output controlled by adjusting the current to the lamp. The entire body of the animal, excluding the treated limb and the head, was covered by a “blanket” of gauze and aluminum foil to prevent unintentional heating. The treatment was monitored by the same hypodermic thermocouples used originally to measure the HIFU temperature. A similar thermocouple was located in the control limb. By monitoring this way, the heat lamp output was continuously fine-tuned to maintain the target temperature of 42°C. Following 2 min at this temperature, the heat lamp was turned off and removed to allow the limb to cool. Unlike the HIFU treatments described above, where the ambient temperature was that of the bath (~37°C), in this case the limbs started out at a more natural level, 2 to 3°C lower. A side-by-side comparison of peak temperatures and thermal doses due to p-HIFU and HT is shown in Fig. 2. Note that the blood pool heating is insignificant during the HT, as shown by the lack of increasing temperature in the control limb.

### Recovery, sectioning and sampling

Following treatment, each mouse was allowed to recover from anesthesia for approximately 20 min before receiving a 100  $\mu\text{l}$  tail vein injection of red fluorescent, polystyrene nanoparticles (Invitrogen Corp., Carlsbad, CA, USA). The suspension of nanoparticles (diameter = 200 nm) was at a stock concentration of  $10^{11}$   $\text{mL}^{-1}$ . The excitation and emission wavelength for the fluorophore was 580 nm and 605 nm, respectively. For one group, this recovery period was extended out to 2, 6 and 24 h ( $n = 6$  each) before injections. Unless otherwise mentioned, the particles were allowed to circulate for 1 h before sacrificing the mouse. Following sacrifice, the remaining particles in the vasculature were flushed by perfusing with saline. The chest cavity of the mouse was opened to expose the heart and liver immediately after sacrifice. The tip of the liver was clipped off, and 10 mL of saline solution was flushed through the animal by slow injection into the left ventricle of the heart. This technique was used in lieu of waiting for the bloodstream to clear normally, and was validated against waiting a 24-h clearing period following injection.

After sacrifice and perfusion, the treated calf muscle was extracted and frozen under a coat of OTC tissue-freezing medium (Fisher Scientific, Fair Lawn, NJ, USA). Cryosections were taken perpendicular to the ultrasonic treatment axis from regular depths at 1 mm intervals, beginning at 0.5 mm from the treatment surface and progressing to the distal side of the leg, typically 5.5 mm. Sections

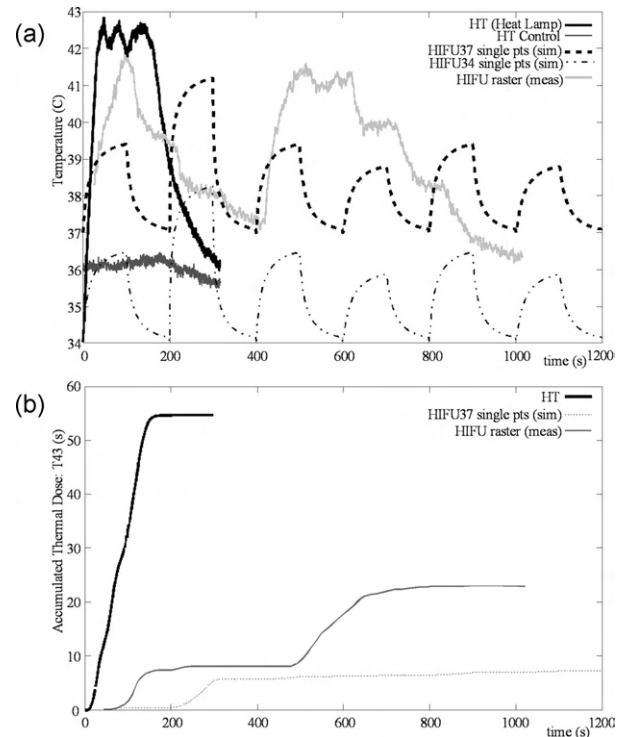


Fig. 2. (a) Temperature vs. time. “HT” shows the temperature of muscle measured during a “heat only” treatment using a heat lamp source; “HT Control” gives the simultaneous temperature measurement from the insulated control limb. Note that ambient limb temperature in air, as demonstrated by the initial temperature of the HT, is actually 34°C, which is lower than the 37°C bath temperature typically used for p-HIFU treatments (see above). “HIFU37” refers to p-HIFU treatment in a 37°C bath; “HIFU34” to p-HIFU treatment in a 34°C bath. Both of these are simulated by extrapolating the measurements of Fig. 1 to predict the heating and cooling of a single point. “HIFU raster” refers to the temperature measured at a given location while a complete treatment is without a cool-down period between raster sites. (b) t43 equivalent thermal dose calculated for these temperature profiles. HT is greater than HIFU37 and HIFU raster in terms of both peak temperature and thermal dose. Note, the thermal dose for HT control and HIFU34 is approximately 0.

were viewed unstained under a fluorescent microscope. Digital images were captured for each section on a  $2 \times 2$  mm grid at  $\times 100$  magnification and a resolution of  $3900 \times 3900$  pixels. The field of view of each image was approximately  $1.36 \text{ mm} \times 1.08 \text{ mm}$  and typically 5 to 8 images could be collected at each depth, depending on the size of the section, for a total of 25 to 40 images per leg. These became the raw data for further processing and analysis. A few cross sectional and surface images were also collected for qualitative analysis.

### Image processing

Images were processed to quantify the overall delivery of particles to the treated tissue and corresponding



Fig. 3. Threshold processing of a typical fluorescent image. Large artifacts (vertical arrows) are recognized and removed from consideration, leaving the area fraction of fine particles (horizontal arrows) as the measure of delivery. Bar = 100  $\mu\text{m}$ .

controls. Using thresholding and particle analysis routines included in ImageJ (National Institutes of Health, Bethesda, MD, USA), the bright pixels were grouped into “fine” (less than 300 pixels in size) and “large” (greater than 300 pixels in size) particles (Fig. 3). Particles greater than 300 pixels in size were excluded from consideration for two reasons. The first was to eliminate brighter regions due to auto-fluorescence, particularly where tissue is folded during sectioning. The second reason was to remove large particle agglomerations, whether due to contamination or occurring in blood vessels or bone marrow, which are also often accompanied by a bloom from saturation of the optics. The particle artifacts were removed at a lower threshold to prevent any noise from their fringes being counted as “fine” particles. Using two thresholds in this way also takes advantage of the sharp intensity gradient in the vicinity of a fluorescent nanoparticle signal compared with the above mentioned artifacts. The measured quantity was the net “fine particle density”, defined as the sum of “fine particle” area divided by the sum of the image area less the artifact area for all images collected from a given sample. Typically, the large particle area fraction represented less than 1% of the total image area.

#### Cavitation studies

Some of the treated animals were specifically designated for cavitation studies. During treatment at 40 W (standard) and also at 20 W, the spectrum of the back-scattered HIFU was measured by use of 2 channels of an HP 4130 network analyzer (Hewlett Packard, Palo Alto, CA, USA). The signal for channel 1 came from the built-in co-axial imaging transducer (10 MHz, 81%

bandwidth) while channel 2 was fed the signal from an HGL hydrophone (Onda Corp., Sunnyvale, CA, USA) aimed in the general direction of the acoustic focus of the HIFU transducer, at an approximate distance of 2 cm between the forward tip of the hydrophone and the axial center of the focus. The first receiver was guaranteed to have accurate spatial targeting but with poor sensitivity at low frequencies; whereas the second receiver has excellent response in the frequency range of interest but might not be perfectly targeted. Spectra collected this way were compared for strength of higher harmonics, half harmonics, and broadband noise levels. Both transducers consistently showed the same trends, the hydrophone data were selected for analysis because of their superior frequency response.

#### Statistical analysis

A nonparametric, paired test (Mann-Whitney) was used to determine whether significant differences occurred between net fine particle density of control and treated tissues for the HIFU exposures in the 37°C bath ( $n = 6$ ) and 34°C bath ( $n = 7$ ) and for the HT treatment ( $n = 6$ ). The same test was used to compare treated and control results for the recovery study. Kruskal-Wallis was used to test for differences in the means.

## RESULTS

#### Heat treatment

In the “standard” HIFU37 treated muscle, the median fine particle area fraction (FPAF) was found to be 0.060%. This was a significant increase ( $p = 0.016$ ) over the control muscle density of 0.030%. The low-temperature HIFU34 treated muscle showed an even larger difference, with a FPAF of 0.18% in the treated side versus 0.028% in the control ( $p = 0.008$ ). Finally, in the HT animals, the FPAF was 0.033%, which is not significantly different ( $p = 0.34$ ) from the control at 0.027%. Results appear in Fig. 4.

#### Recovery following treatment

Following 2 h, 6 h and 24 h recovery, a significantly greater fraction of systemically injected nanoparticles was still detected in the treated muscle compared with the control (Fig. 5). Although an apparent trend was observed where more NPs are found as the recover period was increased, it was not statistically significant ( $p > 0.5$ ).

#### Histology

Besides the quantitative analysis, a number of images were collected for qualitative analysis. Cross-sections showed a much higher distribution of particles at the skin surface and just below, to a depth of less than 0.2 mm, than

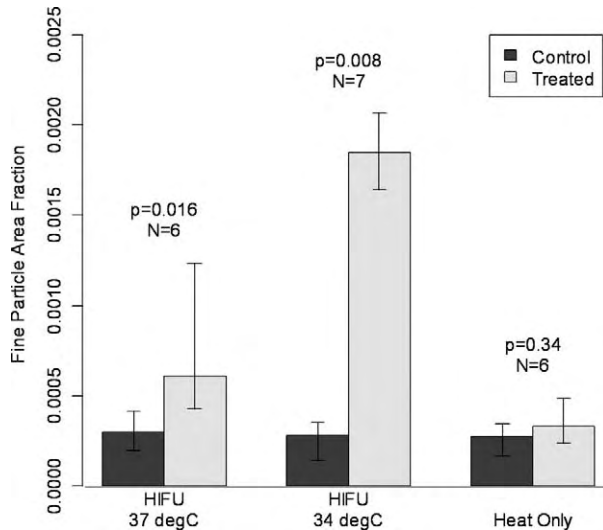


Fig. 4. Comparison of heat treatment (ambient limb temperature at 34°C) to standard p-HIFU treatment with 37°C bath, and low temperature pulsed HIFU treatment with 34°C bath. Despite elevated absolute temperatures and thermal doses relative to the HIFU treatments, the heat-only treatment showed no significant increase in particle delivery. Bars indicate group medians and quartiles.

found in the bulk tissue (Fig. 6). Relatively large deposits of these particles were also found in the bone marrow.

#### Cavitation spectral analysis

Three mice each were treated at 40 W (standard power) and 20 W while constantly monitoring the spec-

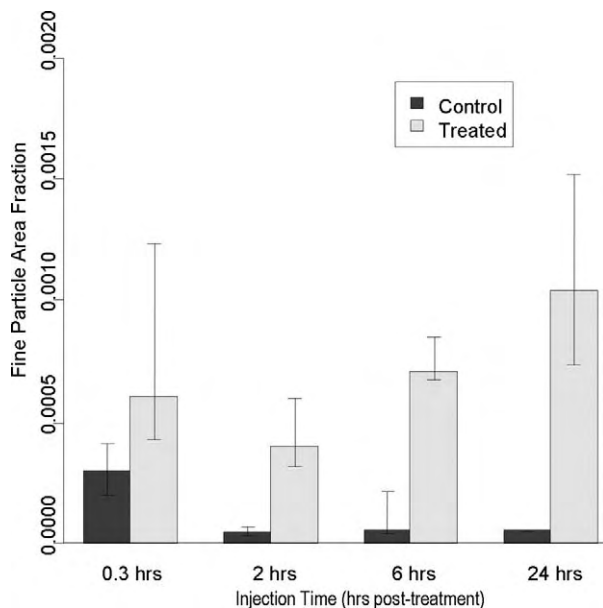


Fig. 5. Longevity of p-HIFU (HIFU37) effects out to 24 h. Particle delivery is not significantly affected by a 24 h waiting period between p-HIFU treatment and tail vein injection. Bars indicate group medians and quartiles.

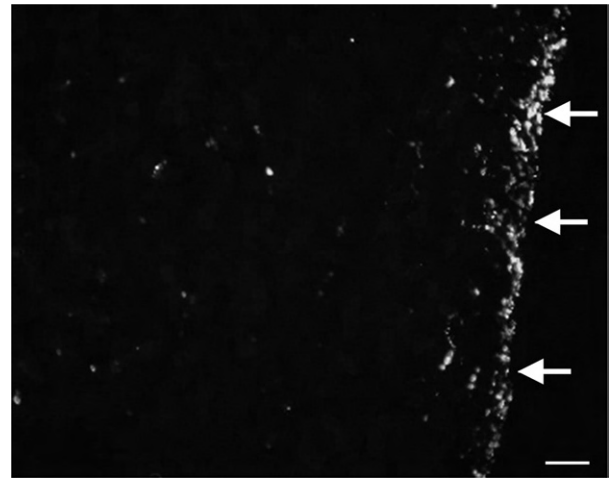


Fig. 6. Cross-section of a p-HIFU treated region, showing muscle surface (arrows right, skin removed). An increase in fluorescent particles is observed near surface. Bar = 100  $\mu$ m.

trum of the backscattered ultrasound. The features that were analyzed at each power level were the harmonic content, the half harmonic content and the broadband noise level. On average, all of these features were distinguishable at both power levels, with some variability between treatment locations on the same leg. Generally, the 20 W power level showed less harmonic distortion and less broadband noise than the 40 W, but relatively more half harmonic content (Fig. 7).

## DISCUSSION AND SUMMARY

The results of this study demonstrate the ability of p-HIFU as a means for increasing targeted macromolecular delivery; however, the mechanisms by which this occurs are less clear. Nanoparticles with a diameter of 200 nm were chosen based on preliminary studies that consistently showed that very small amounts could extravasate across the nonfenestrated endothelium of the microvasculature in the muscle. The goal of this study was to provide preliminary evidence as to the mechanism by which p-HIFU exposures enhance delivery. Experiments were carried out to investigate the potential contributions of the two best known ultrasound mechanisms for producing bio-effects: the generation of heat and acoustic cavitation (O'Brien 2007).

Experiments into the potential effects of a thermal mechanism clearly demonstrated that the hyperthermia accompanying p-HIFU cannot, by itself, explain the observed effects. Hyperthermic drug delivery techniques require tissue to maintain an absolute temperature (typically greater than 39°C) for some period (hours, for temperatures between 39 and 42°C) (Song 1984; Kong et al. 2001), to achieve the desired effect. In our case, we

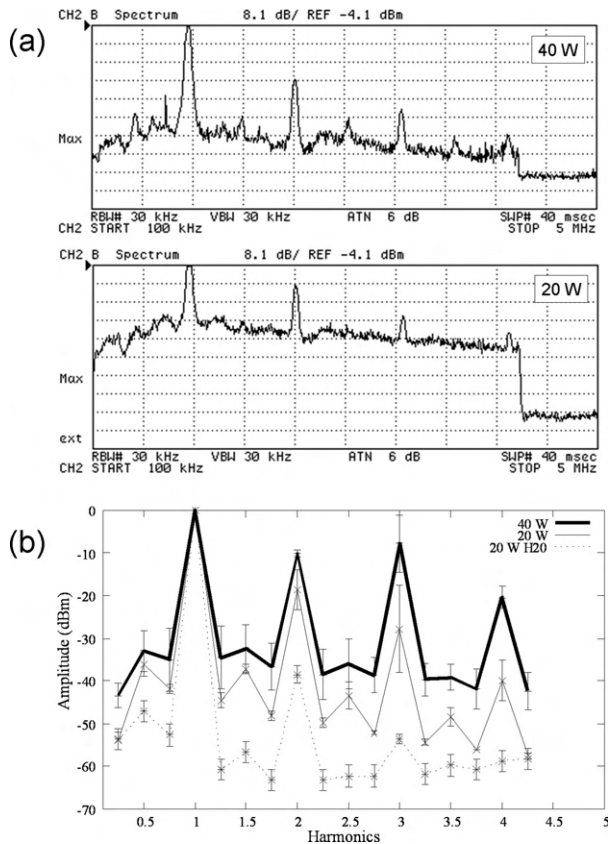


Fig. 7. (a) Spectra collected during treatments at 40 W and 20 W TAP. The spectra give the maximum value measured over 40 pulses, at a single raster point. The trailing edge at far right is outside of the pulse, and thus represents the level of system noise. The sweep runs from 0.1 to 5 MHz and each y division represents 8.1 dB below the reference level of  $-4.1$  dBm. (b) Representation of normalized (with respect to fundamental) spectra at 40 and 20 W TAP; 20 W H<sub>2</sub>O is the spectrum in degassed water for comparison.

demonstrated that the significant increase in nanoparticle delivery produced by our “standard” p-HIFU treatments cannot be reproduced by heating alone, and that significantly lowering the thermal dose of the p-HIFU treatment (achieved by reducing the bath temperature) does not result in a concomitant reduction in delivery.

It is known that local hyperthermia results in a 5- to 10-fold increase in blood flow to muscle (Wust *et al.* 2007; Song 1984), from which one might expect a few fold increase in fluid current across the endothelial wall. These studies have indicated that a thermal tolerance develops and the initial large increase in transport steadily drops back to baseline values within a few hours (Song 1984), even with the temperature remaining elevated. Kong *et al.* (2001) for example showed that enhanced extravasation of nanoparticles due to hyperthermia at 42°C for 1 h is completely reversed within 6 h. In the case of p-HIFU, enhanced transport is maintained

even 24 h following treatment, in stark contrast to the case of hyperthermia.

While we have established that the p-HIFU heating is, by itself, not the cause of increased delivery, the same cannot be said about acoustic cavitation. Part of the ambiguity arises from the size of the animal model. With mice, the dimension of the bulk tissue is very close to the length of the focal zone, making it difficult to avoid surface effects at the skin and bone. In fact, blister-like lesions were often visible at the skin surface during sonication and may have been an indication of cavitation occurring there. Our prior studies in tumors have indicated that some hemorrhage is observed at the surface with the skin and in the connective tissue next to the bone, at 40 W TAP, although not consistently at 20 W (O’Neill *et al.* 2006). This would appear to be consistent with spectral results of the present study, which seem to indicate the presence of inertial cavitation at 40 W TAP, with relatively less inertial and more noninertial cavitation at 20 W TAP, in the vicinity of the focus. However, histologic analysis of the bulk tissue showed little or no extravasation of erythrocytes or other structural alterations that may be associated with acoustic cavitation.

The recovery time from (noninertial) cavitation induced opening of the blood-brain barrier is on the order of a few hours (Hynynen *et al.* 2005), being substantially less than the more than 24 h observed in the present study. It might be the case therefore, that cavitation is occurring only in select regions (*e.g.*, at tissue interfaces) and is not a major contributor to the particle delivery. Experiments are presently being planned in larger animal models, where greater confidence can be achieved that any spectral indications are not coming from surface effects and other interfaces (*e.g.*, soft tissue and bone).

Inertial cavitation can be employed as potent mechanism for enhancing delivery through the process of sonoporation. Here, the wall direct re-entrant jet occurring from asymmetrical collapse of a cavitating bubble at a cell surface can temporarily permeabilize the membrane, allowing for increased uptake of DNA or other agents in a nondestructive manner. This type of enhanced delivery occurs only at the cellular level, where membranes typically remain open for only a number of seconds (Deng *et al.* 2004). It, therefore, requires administration of agents to be delivered before exposures and so is not relevant to the present study, where enhanced delivery occurred up to 24 h after exposures.

If neither of the two leading candidates, hyperthermia or cavitation, mediates the therapeutic effects of p-HIFU, lesser known possibilities must be considered, such as purely mechanical effects. In this case, the tissue is treated essentially as an inert material, at least on the timescale of the interaction. Thus, only the physical forces carried by the p-HIFU wave itself need be con-

sidered important. These forces come in two varieties: the dynamic, oscillating pressures and temperatures that accompany the propagating wave; and the quasi-static radiation forces due to momentum transfer between the decaying wave and the absorbing material. While the first is proportional to the ultrasonic displacement, the second is proportional to the ultrasonic intensity, or the square of the ultrasonic displacement (Lizzi et al. 2003), which can be on the order of tens of microns for the exposures used in the present study (Frenkel et al. 2005, 2006b). This displacement also has a measurable shear component, which some researchers have linked to tissue changes (Frenkel et al. 2000a; Tesfamariam and DeFelicce 2007) that can enhance nanoparticle transport (Frenkel et al. 2000b).

An unexpected result of the study was found when lowering the bath temperature from 37 to 34°C during p-HIFU treatment. If the p-HIFU enhanced delivery was due strictly to hyperthermia, the expected result would be a very significant reduction in delivery as the thermal dose is dropped essentially to zero. Instead, a significant increase occurred. One hypothesis is that the higher temperature bath (37°C) increases perfusion to all peripheral musculature, reducing the relative impact of the p-HIFU treatment by shunting the particles to other locations. However, this argument would have been more convincing had the drop in delivery to the treated limb been accompanied by a measurable increase in delivery to the control limb, which was not observed. Another possibility is that a change in tissue properties occurred at the lower temperature, which has been previously reported. Hrapko et al. (2008), for example, found that lowering tissue temperature from 37°C to room temperature can stiffen its response to shear deformation. These results support those previously found, where shear stiffness in skeletal muscle and other soft tissues (e.g., liver) increased proportionally with decreasing temperature from 45 to 15°C (Kruse et al. 2000). If relevant changes of this nature occurred when the temperature was dropped from 37 to 34°C in the present study, it could conceivably have rendered the tissue, in effect, less compliant, and more liable to structural alterations (i.e., enlargement of gaps between endothelial cells), which in turn would increase extravasation. More in-depth study of this phenomenon in the future may in turn be the basis for validating the potential role of radiation force induced displacements as a viable mechanism for enhancing tissue permeability.

In conclusion, while the results of the present study indicate that a thermal mechanism does not contribute to the observed enhancement in nanoparticle delivery, the same cannot be said in regards to acoustic cavitation. Preliminary evidence, however, does seem to suggest that a third, and not previously described, mechanism (i.e., acoustic radiation force induced displacements) may also be playing a part. Further investigations will have to be carried out to

make these determinations. A better understanding of the mechanisms by which p-HIFU enhanced delivery occurs will ultimately contribute to facilitating the process of optimizing these exposures for this purpose.

*Acknowledgments*—The authors thank Dr. Matthew R. Dreher for thoughtfully providing insights into the complexities of drug delivery, some of which are addressed in this manuscript and Dr. Bradford J. Wood for support of this work. We also thank Ms. Hilary Hancock for editing the manuscript and providing helpful editorial suggestions. The work was done under the auspices of the Research Associateship Program of the National Academies of Sciences, and was supported in part by the intra-mural research program of the Clinical Center, National Institutes of Health.

## REFERENCES

- Clarke RL, ter Haar, GR Temperature rise recorded during lesion formation by high-intensity focused ultrasound *Ultrasound Med Biol* 1997;23:299–306.
- Deng CX, Sieling F, Pan H, Cui J. Ultrasound-induced cell membrane porosity *Ultrasound Med Biol* 2004;30:519–526.
- Dittmar KM, Xie J, Hunter F, Trimble C, Bur M, Frenkel V, Li KC. Pulsed high-intensity focused ultrasound enhances systemic administration of naked DNA in squamous cell carcinoma model: Initial experience. *Radiology* 2005;235:541–546.
- Frenkel V, Kimmel E, Iger Y. Ultrasound-induced intercellular space widening in fish epidermis. *Ultrasound Med Biol* 2000a;26:473–480.
- Frenkel V, Kimmel E, Iger Y. Ultrasound-facilitated transport of silver chloride (AgCl) particles in fish skin. *J Control Release* 2000b;68:251–261.
- Frenkel V, Deng C, Quijano J, Stone MJ, Dromi S, Hunter F, Xie J, Wood BJ, Li KCP, O'Neill BE, Quinn TP. Pulsed-high intensity focused ultrasound (HIFU) exposures for enhanced delivery of therapeutics: Mechanisms and applications. In: *Proceedings of the 5<sup>th</sup> International Symposium on Therapeutic Ultrasound*. Boston, MA: AIP, 2005.
- Frenkel V, Etherington A, Greene M, Quijano J, Xie J, Hunter F, Dromi S, Li KC. Delivery of liposomal doxorubicin (Doxil) in a breast cancer tumor model: Investigation of potential enhancement by pulsed-high intensity focused ultrasound exposure. *Academic Radiol* 2006a;13:469–479.
- Frenkel V, Oberoi J, Stone MJ, Park M, Deng C, Wood BJ, Neeman Z, Horne M 3rd, Li KC. Pulsed high-intensity focused ultrasound enhances thrombolysis in an *in vitro* model. *Radiology* 2006b;239:86–93.
- Order MM, Barnett SB, Vella GJ, Edwards MJ, Wood AK. *In vivo* heating of the guinea-pig fetal brain by pulsed ultrasound and estimates of thermal index. *Ultrasound Med Biol* 1998;24:1467–1474.
- Hrapko M, van Dommelen JA, Peters GW, Wismans JS. The influence of test conditions on characterization of the mechanical properties of brain tissue. *J Biomech Eng* 2008;130:031003.
- Hynynen K. The threshold for thermally significant cavitation in dog's thigh muscle *in vivo*. *Ultrasound Med Biol* 1991;17:157–169.
- Hynynen K, McDannold N, Sheikov NA, Jolesz FA, Vykhodtseva N. Local and reversible blood-brain barrier disruption by noninvasive focused ultrasound at frequencies suitable for trans-skull sonications. *NeuroImage* 2005;24:12–20.
- Kennedy JE. High-intensity focused ultrasound in the treatment of solid tumors. *Nat Rev Cancer* 2005;5:321–327.
- Khaibullina K, Jang BS, Sun H, Le N, Yu S, Frenkel V, Carrasquillo JA, Pastan I, Li KC, Paik CH. Pulsed high intensity focused ultrasound enhances uptake of radiolabeled monoclonal antibody to human epidermoid tumor in nude mice. *J Nucl Med* 2008;49:295–302.
- Kong G, Braun RD, Dewhirst MW. Characterization of the effect of hyperthermia on nanoparticle extravasation from tumor vasculature. *Cancer Res* 2001;61:3027–3032.
- Kruse AS, Smith JA, Lawrence AJ, Dresner MA, Manduca A, Greenleaf JF, Ehman RL. Tissue characterization using magnetic reso-

- nance elastography: Preliminary results. *Phys Med Biol* 2000;45:1579–590.
- Lizzi FL, Muratore R, Deng CX, et al. Radiation-force technique to monitor lesions during ultrasonic therapy. *Ultrasound Med Biol* 2003;29:1593–1605.
- Miller DL, Song J. Tumor growth reduction and DNA transfer by cavitation-enhanced high-intensity focused ultrasound *in vivo*. *Ultrasound Med Biol* 2003;29:887–893.
- O'Brien WD Jr. Ultrasound-biophysics mechanisms. *Prog Biophys Mol Biol* 2007;93:212–255.
- O'Neill BE, Quinn TP, Frenkel V, Li KCP. A multi-phasic continuum damage mechanics model of mechanically induced increased Permeability in Tissues. In: Bushby AJ, Ferguson VL, Ko C, Oyen ML, eds. *Mechanical Behavior of Biological and Biomimetic Systems* (Mater. Res. Soc. Symp. Proc. 898E) Warrendale, PA, 2005: 0898-L02–05.
- O'Neill BE, Frenkel V, Li KCP, Quinn TP. Pulsed HIFU for enhanced drug delivery: A study of possible mechanisms. *Proc Intl Sym Ther US*. In: *Proceedings of the 6<sup>th</sup> International Symposium on Therapeutic Ultrasound*. Oxford: AIP, 2006.
- Patel P, Luk A, Durrani AK, Dromi S, Angstad M, Wood BJ, Frenkel V. *In vitro* and *in vivo* evaluations of increased spatial heat deposition using a split focus high intensity ultrasound (HIFU) transducer. *Int J Hyperthermia* 2008;24:537–549.
- Quijano J, Colunga A, Xie J, Frenkel V, Li K. Enhanced regression in a squamous cell carcinoma murine tumor model using pulsed-high intensity focused ultrasound (HIFU) and naked TNF- $\alpha$  plasmid. *Proceedings of the 4th Annual Meeting of the Society for Molecular Imaging*. Cologne, 2005.
- Sapareto SA, Dewey WC. Thermal dose determination in cancer therapy. *Int J Radiat Oncol Biol Phys* 1984;10:787–800.
- Song CW. Effect of local hyperthermia on blood flow and microenvironment: a review. *Cancer Res* 1984;44(10 Suppl.):4721s–4730s.
- Stone MJ, Frenkel V, Dromi S, Thomas P, Lewis RP, Li KCP, Horne M, Wood BJ. Pulsed-high intensity focused ultrasound enhanced tPA mediated thrombolysis in a novel *in vivo* clot model, a pilot study. *Thromb Res* 2007;121:193–202.
- Tesfamariam B, DeFelice AF. Endothelial injury in the initiation and progression of vascular disorders. *Vascul Pharmacol* 2007;46:229–237.
- Wu J, Du G. Temperature elevation generated by a focused gaussian beam of ultrasound. *Ultrasound Med Biol* 1990;16:489–498.
- Wust P, Nadobny J, Szimtenings M, Stetter E, Gellermann J. Implications of clinical RF hyperthermia on protection limits in the RF range. *Health Physics* 2007;92:565–573.
- Yuh EL, Shulman SG, Mehta SA, Xie J, Chen L, Frenkel V, Bednarski MD, Li KCP. Delivery of systemic chemotherapeutic agent to tumors by using focused ultrasound: study in a murine model. *Radiology* 2005;234:431–437.

## APPENDIX 1

The accepted thermal heat transfer equation for biological tissues can be written (Wu and Du 1990):

$$c_v \dot{T} = K \nabla^2 T - \frac{c_v}{\tau} T + q_v \quad (\text{A-1})$$

where  $T$  is the rise in temperature,  $K$  is the thermal conductivity,  $c_v$  is the heat capacity,  $\tau$  is the perfusion time constant governing the loss of heat into the bloodstream, and  $q_v$  is the external heat input. In our case, the heat

is deposited in short ultrasonic pulses. Assuming the ultrasonic beam in the focal plane may be approximated as a Gaussian, that is:

$$I(r) \approx I_0 \exp\left(-\frac{r^2}{R^2}\right); \quad (\text{A-2})$$

then:

$$q_v(r) = 2\alpha I(r) \approx 2\alpha I_0 \exp\left(-\frac{r^2}{R^2}\right) \quad (\text{A-3})$$

The error introduced by using Gaussian approximation for the heat source is small compared to the error introduced by approximating the tissue as homogeneous (Wu and Du 1990).

During the ultrasonic pulse, the final term dominates eqn A-1. That is, we can approximate eqn A-1 as:

$$\dot{T}(r, t) \approx \frac{2\alpha I(r)}{c_v} \quad (\text{A-4})$$

Following the  $n$ th pulse, we have:

$$T(r, t_n) = A \exp\left(-\frac{r^2}{R^2}\right) \Delta t_{on} + T(r, t_{n-1} + \Delta t_{off}); \quad A = \frac{2\alpha I_0}{c_v} \quad (\text{A-5})$$

When the first pulse is turned off, at time  $t_1$ , eqn A-1 becomes:

$$\dot{T}(r, t) = \frac{4K}{c_v} \nabla^2 T(r, t) - \frac{1}{\tau} T(r, t) \quad (\text{A-6})$$

With a Gaussian initial condition like eqn 5, an exact solution may be written as:

$$T(r, t) = \frac{A}{1 + B(t - t_1)} \exp\left(\frac{-r^2}{R^2(1 + B(t - t_1))}\right) \exp\left(-\frac{(t - t_1)}{\tau}\right); \quad B = \frac{4K}{c_v R^2} \quad (\text{A-7})$$

Presuming that this decay continues through the next  $N-1$  pulses, and taking advantage of the linearity of the equations, the temperature decay following the  $N$ th pulse may be written:

$$T(r, t) = A \Delta t_{on} \sum_{n=1}^N \exp\left(\frac{-r^2}{R^2(1 + B(t - t_n))} - \frac{t - t_n}{\tau}\right) (1 + B(t - t_n))^{-1} \quad (\text{A-8})$$

where  $t_n$  is the time when the  $n$ th pulse is turned off, that is,  $t_n = n(\Delta t_{on} + \Delta t_{off}) - \Delta t_{off}$ .

Note,  $A$ ,  $B$ ,  $R^2$  and  $\tau$  were all found by fitting  $T(r, t)$  to the data shown in Fig. 1, (ie. simultaneously fitting to all six curves). For the three samples fit (see Table 1), their values are:

dx	dy	A	B	$R^2$	$\tau$
-1.128	-2.013	5.476	0.1571	10.69	105.3
-0.1264	0.1956	20.55	1.051	1.899	69.93
0.0739	0.6211	13.86	1.079	2.443	181.8

dx and dy are the coordinates of the thermocouple relative to the upper left hand focal zone (Fig. 1), and were also extracted from the fit.  $r^2 = (x_n + dx)^2 + (y_n + dy)^2$ , where  $x_n$  and  $y_n$  depend on the particular focal zone in question (1 to 6).